Electronic Supplementary Material (ESI) for Journal of Materials Chemistry A.
This journal is © The Royal Society of Chemistry 2020

Electronic supplementary information

Electrolyte-phobic carbon nanotube current collector for high-voltage foldable lithium-ion battery

Ke Wen Mu [a], Kai Xi Liu [a], Zhi Yong Wang [a], Shahid Zanman [b], Yan Hong Yin [a], Xian Bin Liu [a]*, Ye Sheng Li [a], Bao Yu Xia [b]*, and Zi Ping Wu [a]*

[a] School of Materials Science and Engineering, Jiangxi University of Science & Technology (JXUST), Ganzhou 341000, P. R. China.

[b] Key Laboratory of Material Chemistry for Energy Conversion and Storage (Ministry of Education), Hubei Key Laboratory of Material Chemistry and Service Failure, School of Chemistry and Chemical Engineering, Wuhan National Laboratory for Optoelectronics, Huazhong University of Science and Technology (HUST), 1037 Luoyu Road, Wuhan 430074, P. R. China.

* Corresponding author E-mail: xianbin_liu@jxust.edu.cn (X. B. Liu); byxia@hust.edu.cn (B. Y. Xia); wuziping724@jxust.edu.cn (Z. P. Wu)

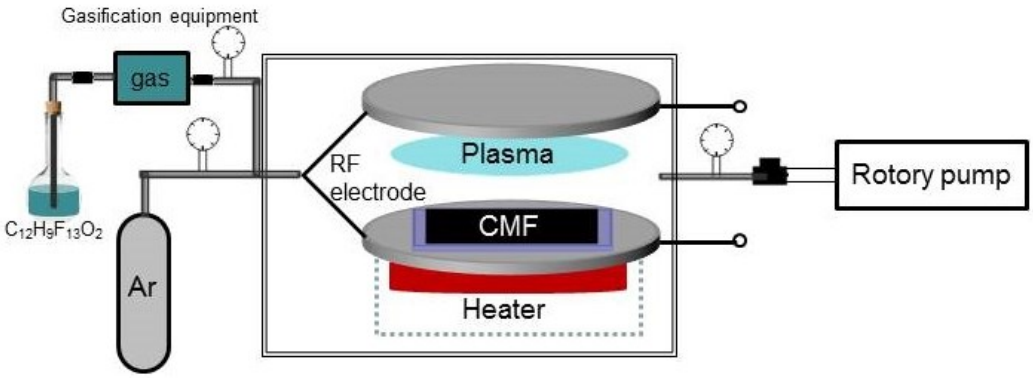

Figure S1. The preparation schematic diagram of electrolyte-phobic CCMF.

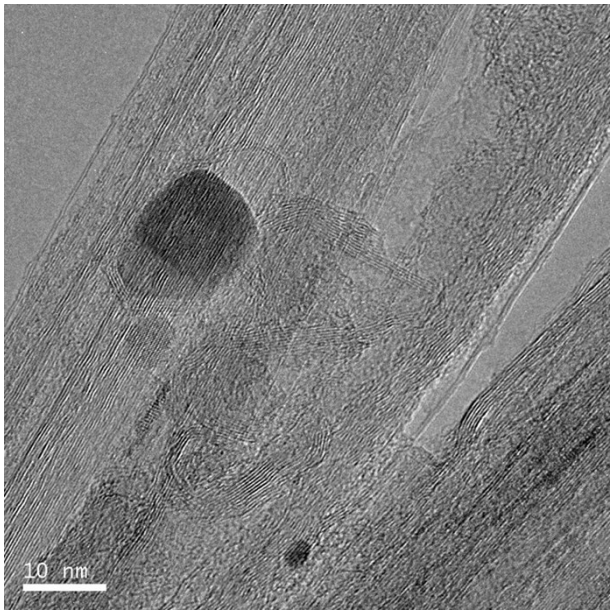

Figure S2. TEM image of CNTs in the CMF.

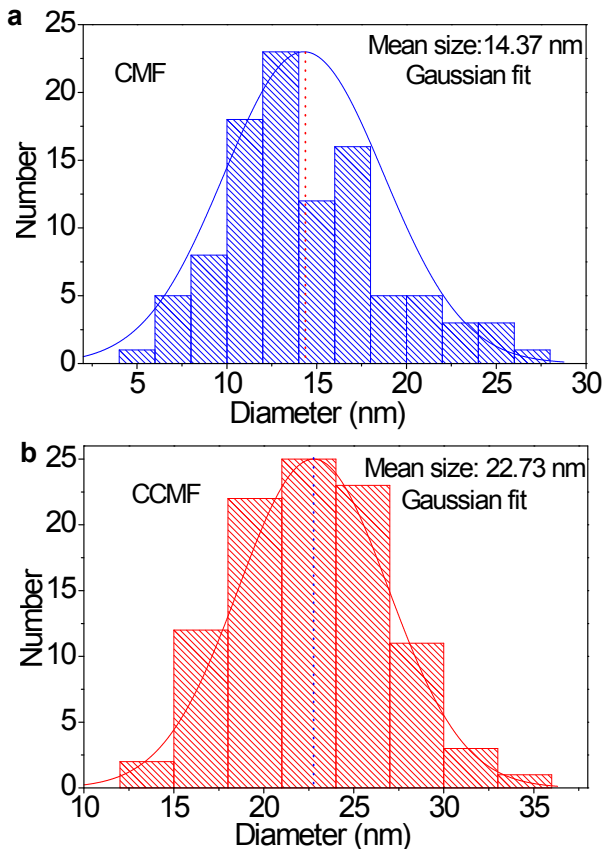

Figure S3. Diameter distributions of CNTs in CMF (a) and CCMF (b).

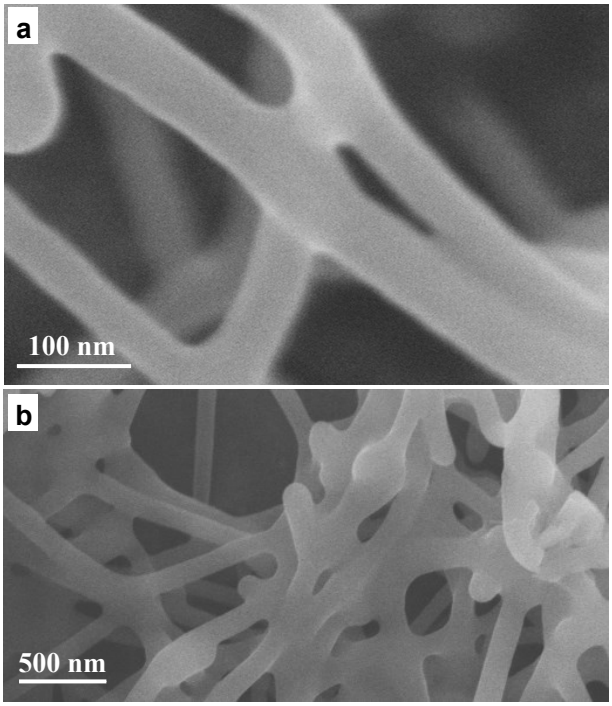

Figure S4. SEM images of CCMF modified by FAS with different time 30 mins (a) and 60 mins (b).

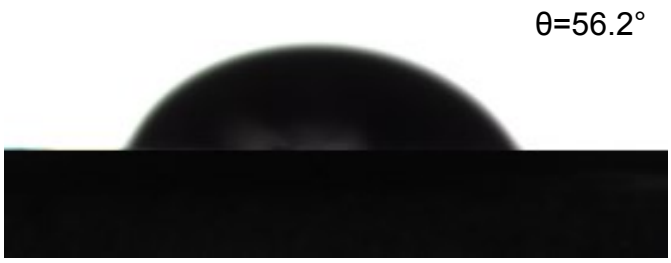

Figure S5. Contact angle of an electrolyte droplet (~4 μL) placed on the surface of CCMF by evaporating FAS directly without inducing plasma.

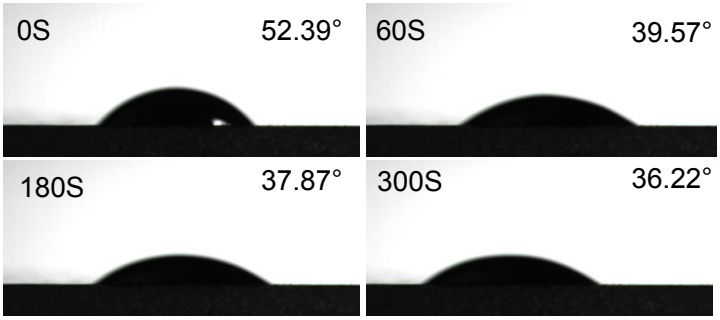

Figure S6. The wettability evaluations of Gra slurry on the CMF current collectors at, 0 s (a), 60 s (b), 180 s (c), 300 s (d).

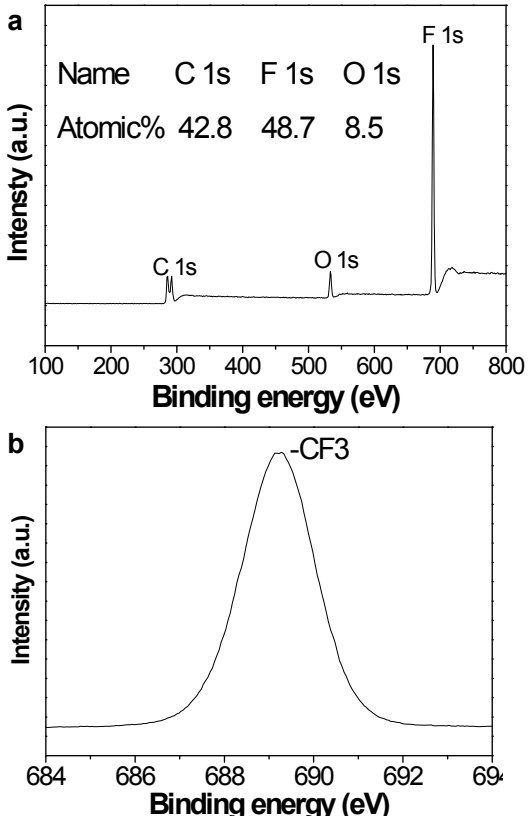

Figure S7. Wide-scan (a), and the corresponding F1s XPS spectra (b)of the CCMF.

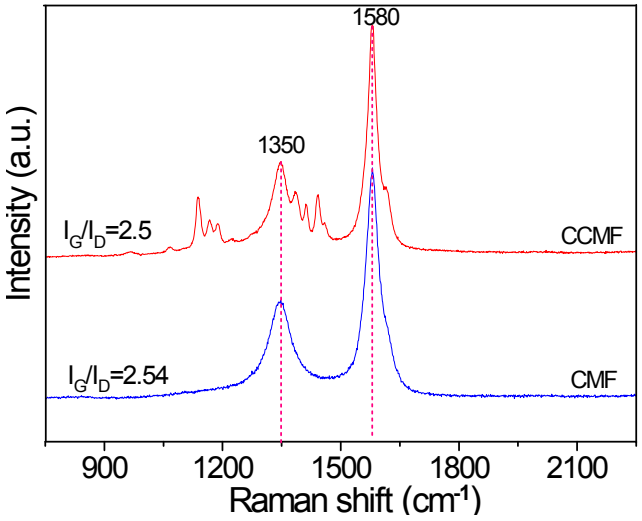

Figure S8. Raman spectra of CMF and CCMF.

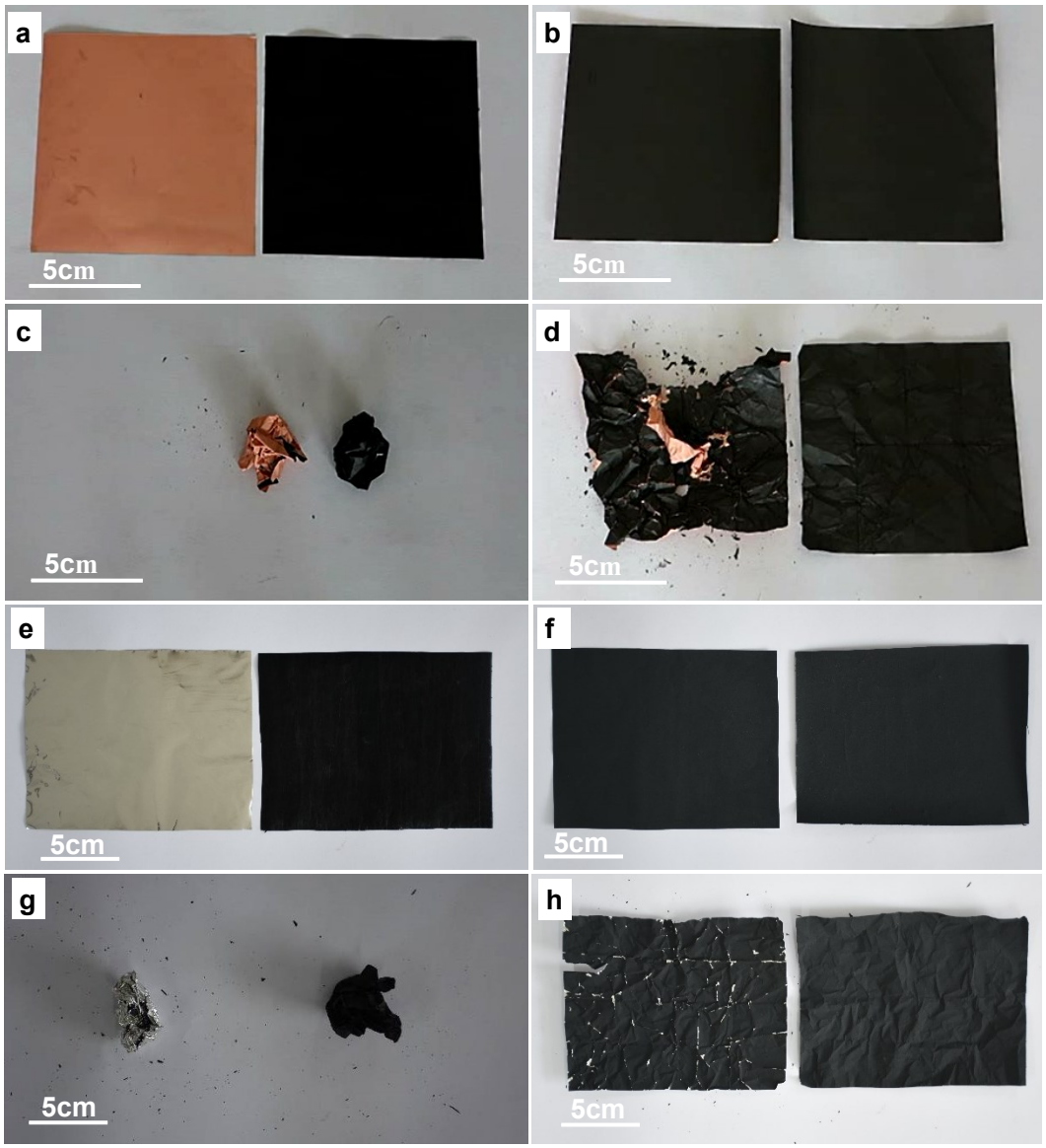

Figure S9. Foldability tests of Cu foil and CCMF based electrodes, Cu foil and CCMF (a), Gra coated Cu foil and CCMF (b). Cu-Gra and CCMF-Gra were deformed (c) and spread out (d). Al foil and, LCO coated on Al foil (e) and CCMF (f), Al-LCO and CCMF-LCO electrodes were deformed (g) and spread out (h).

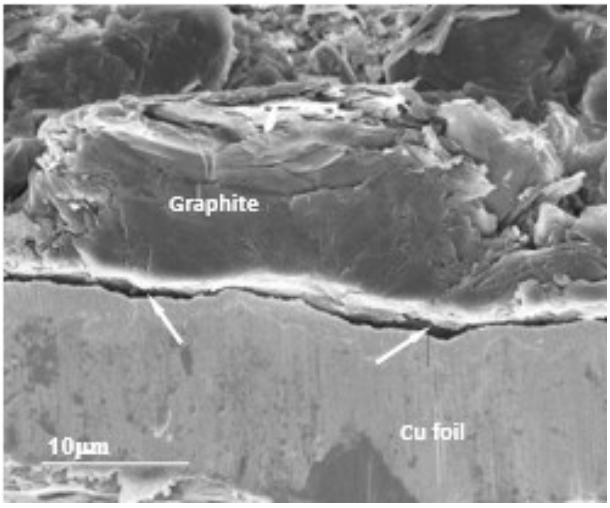

Figure S10. The SEM image of the **c**ross-section of the Cu-Gra interface.

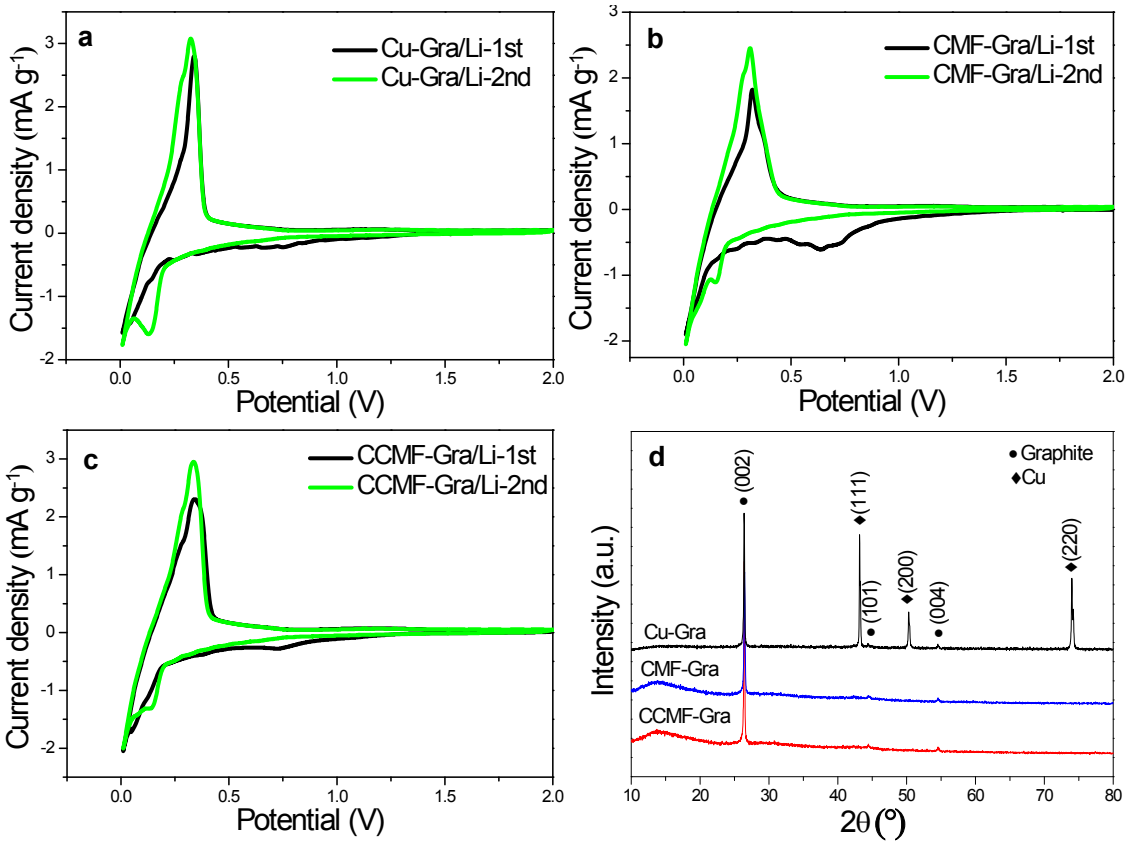

Figure S11. CV curves for the Cu- (a), CMF- (b) and CCMF- (c) based half cells at the first and second cycle. XRD patterns of the Gra surface of the Cu-Gra, CMF-Gra and CCMF-Gra electrodes after first discharging (d).

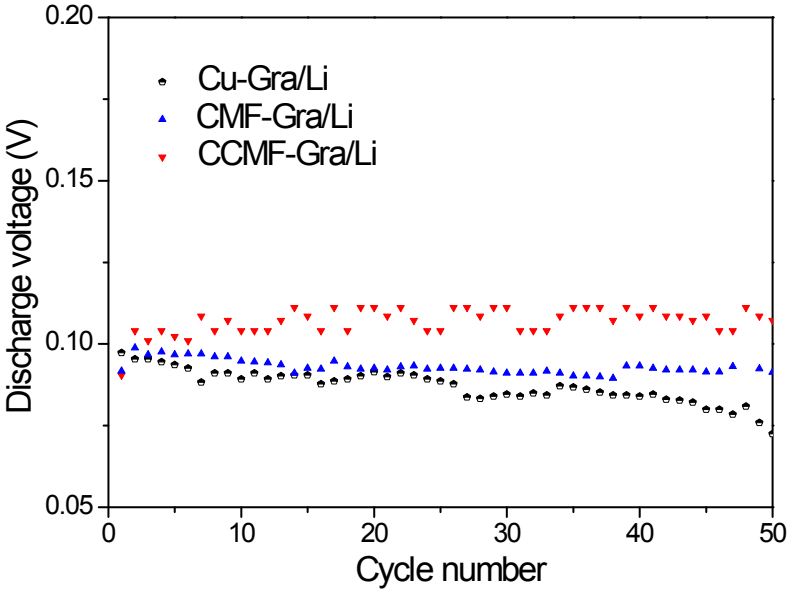

Figure S12. The evolution of the voltage profiles of the half cells based on the CCMF, CMF and metallic current collectors.

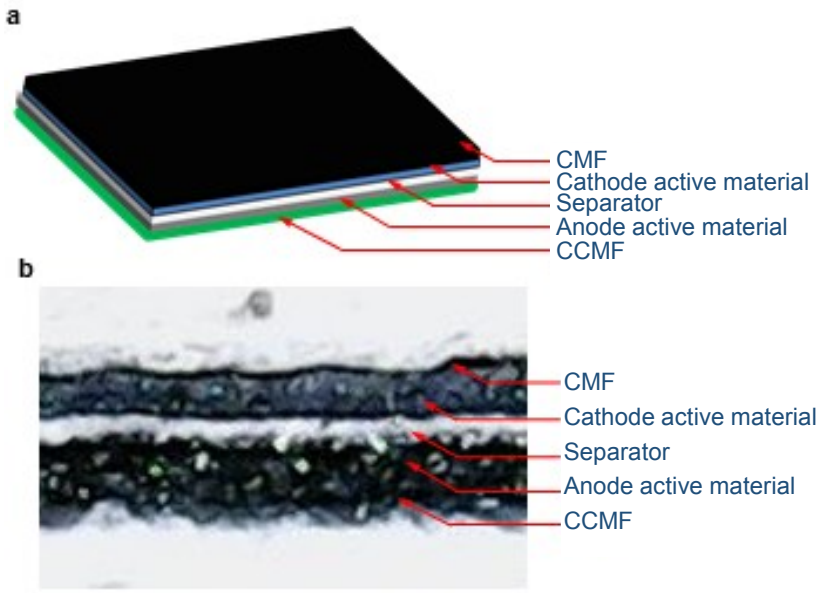

Figure S13. Schematic diagram (a) and photographic prototype (b) of the foldable lithium-ion battery.

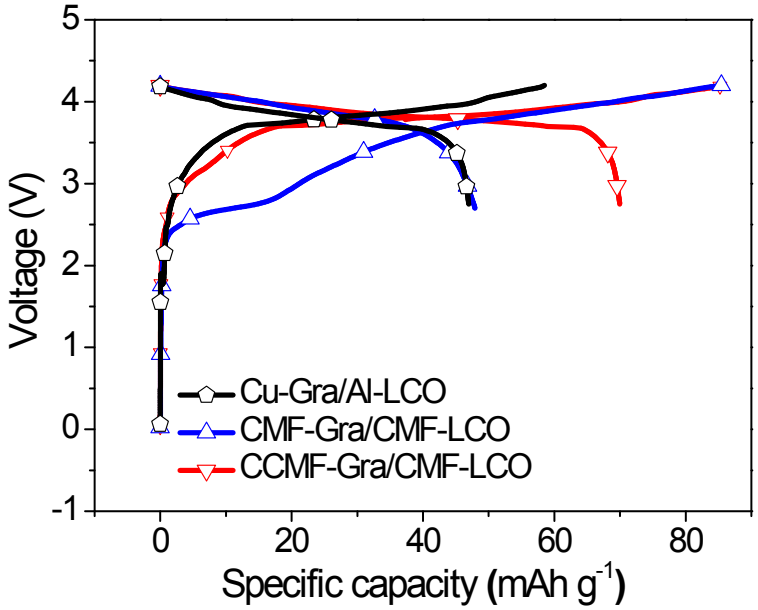

Figure S14. The galvanostatic charge/discharge of FLIBs at the first cycle based on CMF, CCMF and metallic current collectors, the galvanostatic charge/discharge calculated by the weight of the two electrodes. The mass loading of LCO in different electrodes is 15 mg cm^{-2}.

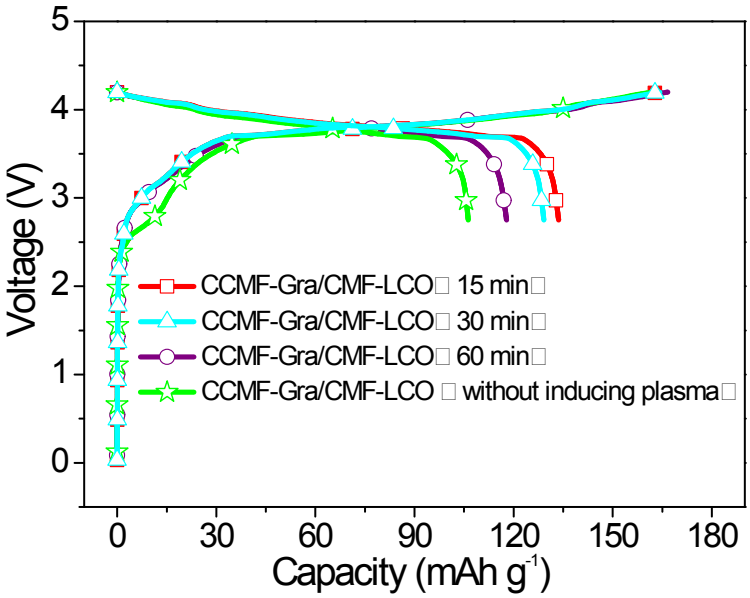

Figure S15. Galvanostatic charge/discharge of the full batteries at the first cycle based on CCMF with different deposition time by PECVD method or modified by FAS without inducing plasma at C-rates of 0.1 C. The Gra mass loading was 7.5 mg cm^{-2}.

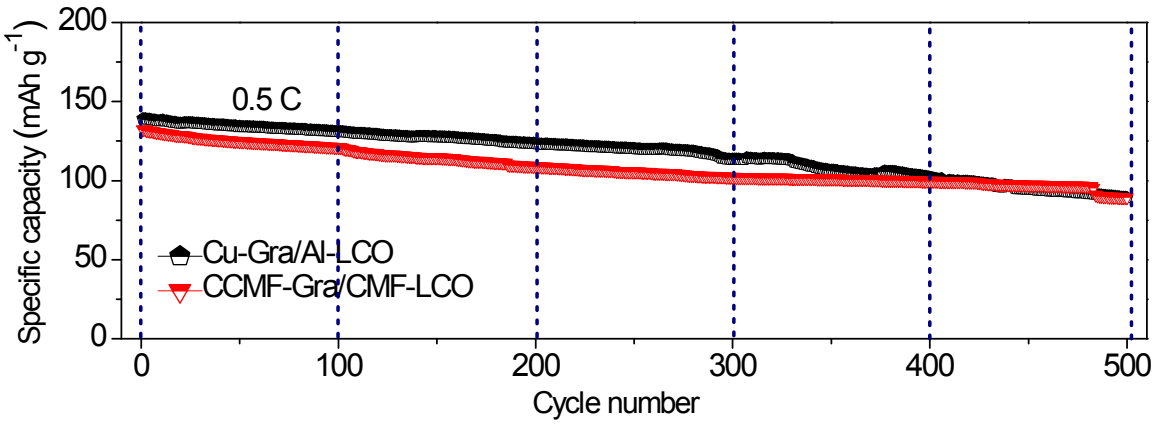

Figure S16. Cycling behaviors of the Cu-Gra/Al-LCO and CCMF-Gra/CMF-LCO batteries at 0.5C, the LCO mass loading was 15 mg cm^{-2}.

The battery of CCMF-Gra/CMF-LCO achieves a stable performance over 500 cycles (capacity retention of 70% at 500th cycle from initial capacity of ~134 mAh g^{-1}), which demonstrate a similar electrochemical performance to commercial battery with metallic current collectors.

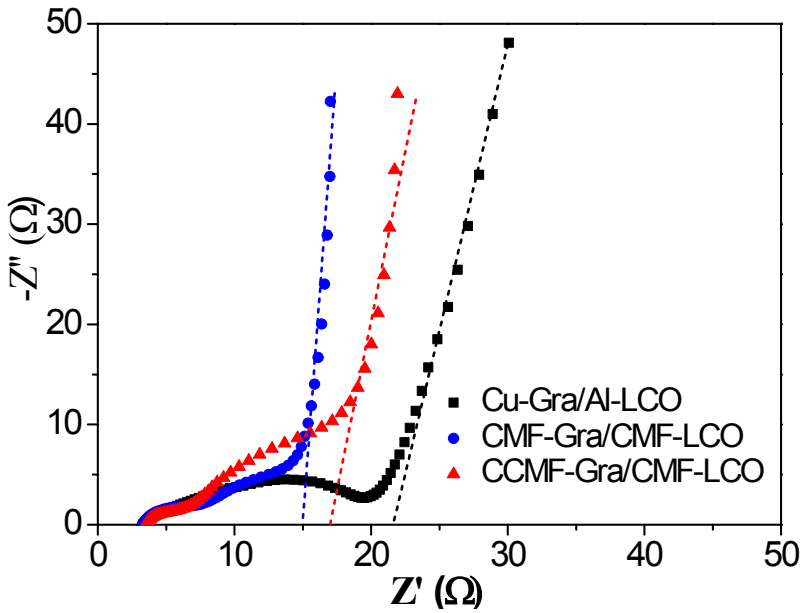

Figure S17. Nyquist plots of the full cells based on CMF, CCMF and metallic current collectors.

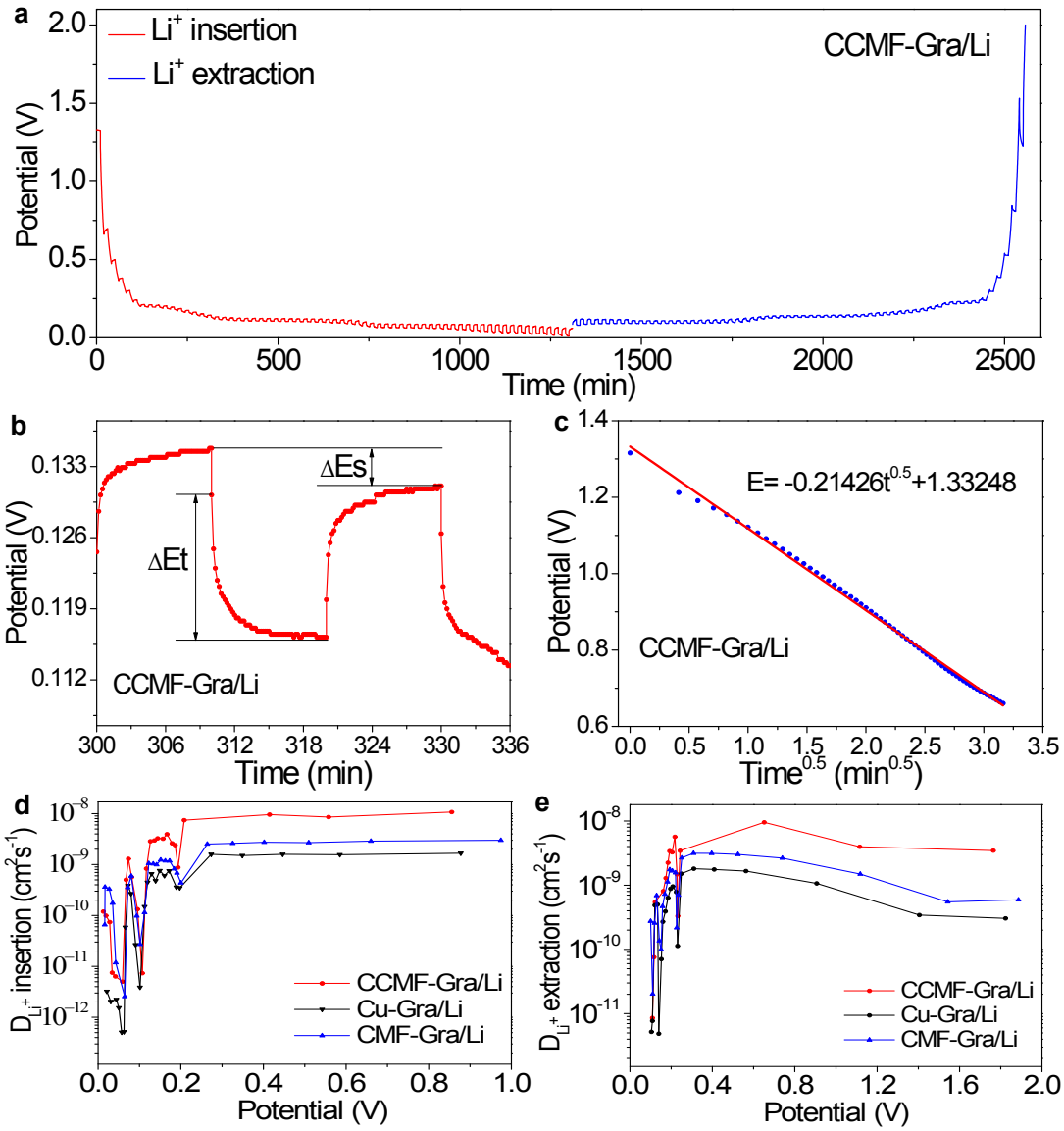

Figure S18. GITT test of the CCMF, CMF and Cu based cells, (a) first cycle GITT curves at 0.1 C, (b), E vs t in a single step, (c) linear relationship between E and $t^{0.5}$ during a typical titration, and (d) insertion and (e) extraction of D_{Li^+} values calculated from the GITT curves for the cells based different current collectors.

To study the Li^+ diffusivity of Gra using different current collectors (CCMF, CMF and Cu), the galvanostatic intermittent titration technique (GITT) experiment was performed on electrode CCMF-Gra during the first Li^+ insertion/extraction processes at room temperature (Figure S18 a). The Li^+ diffusion coefficient (D_{Li}) can be determined using the Fick's second law with equation (1):[1, 2]

$$D_{Li} = \frac{4}{\pi}\left(\frac{m_B V_m}{M_B S}\right)^2 [\frac{\Delta Es}{t\left(\frac{dEt}{d\sqrt{t}}\right)}]^2 \quad (t \ll \frac{L2}{D_{Li}}) \qquad (1)$$

where M_B is the molar weight of Gra, S is the realsurface area of Gra, Vm is the molar volume of Gra, m_B is the mass weight of Gra, t is the titration time, ΔEt is the potential variation during the pulse, and ΔEs is the variation in the equilibrium potential (Figure S18b). Since the potential was linearly proportional to $t^{0.5}$during the single titration (Figure S18c), equation (1) was simplified as equation (2):

$$D_{Li} = \frac{4}{\pi t}\left(\frac{m_B V_m}{M_B S}\right)^2 \left(\frac{\Delta Es}{\Delta Et}\right)^2 (t \ll \frac{L2}{D_{Li}}) \qquad (2)$$

Based on the calculation, the CCMF-Gra /Li, CMF-Gra /Li and Cu-Gra /Li cell variation tendencies of D_{Li} during the Li^+ insertion/extraction processes are shown in Figure S18d, e.

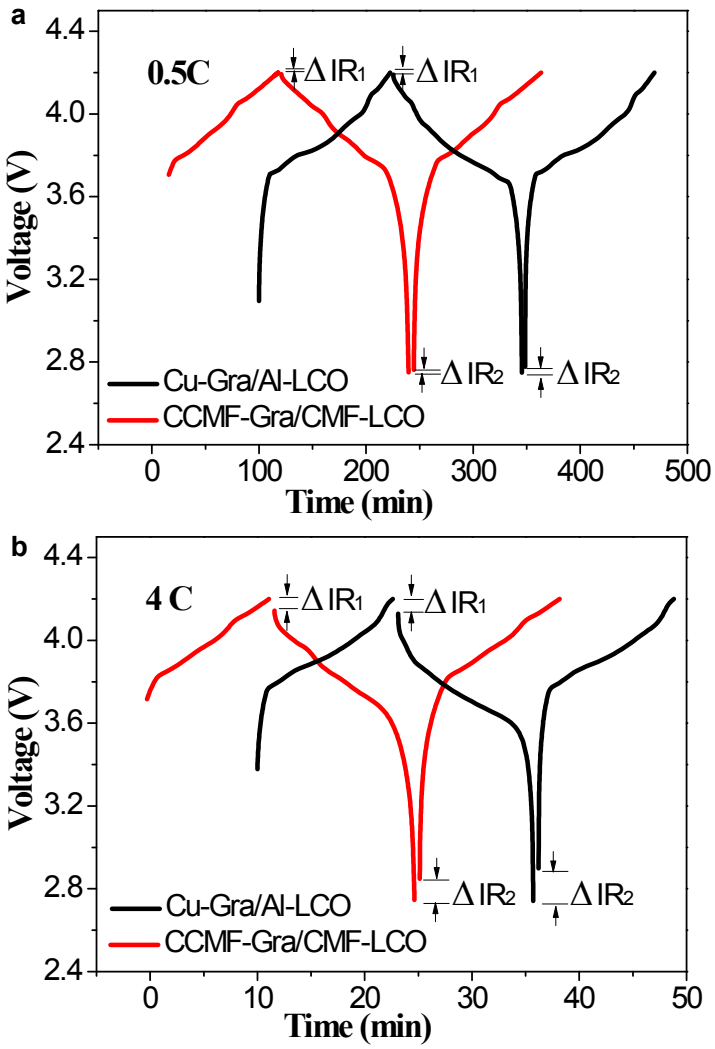

Figure S19. Galvanostatic charge/discharge of the Cu-Gra/Al-LTO and CCMF-Gra/CMF-LTO batteries at charge/discharge rates of ~0.5 C (a) and ~4 C (b), the LCO mass loading was 15 mg cm^{-2}.

Figure S20. Open-circuit voltage of the CCMF-Gra/CMF-LCO battery with small size of 3 cm × 3.5 cm between the flat (a) and foldable (b, c) states.

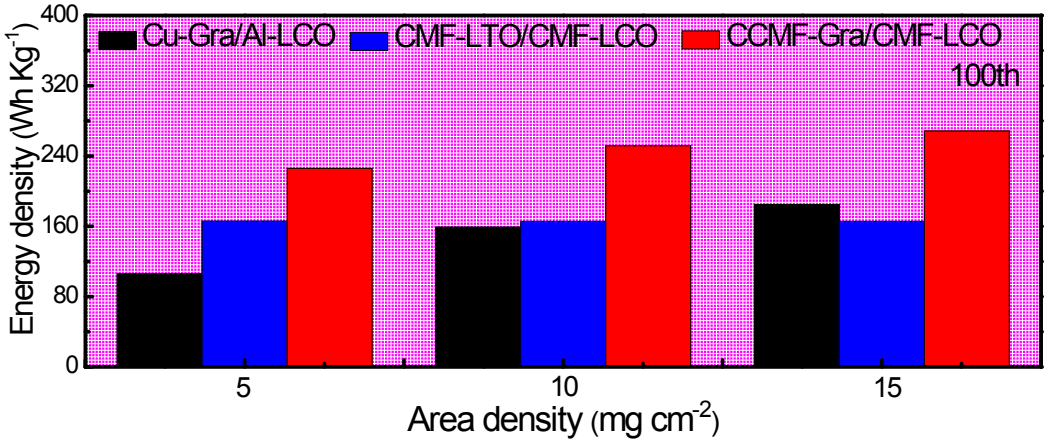

Figure S21. Energy density comparison of the different batteries after charging/discharging 100 times for three different mass loadings of the electrodes, the energy density was calculated by the weight of the two electrodes. All configurations were tested at the same C-rate of 0.5 C.

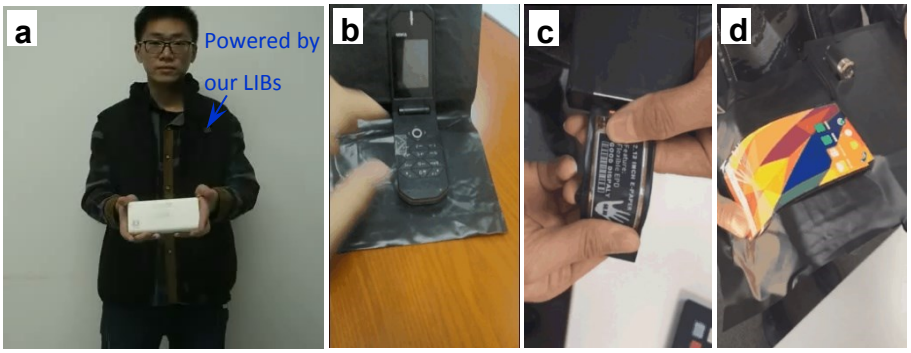

Figure S22. Popular electronics driven by this high voltage battery.

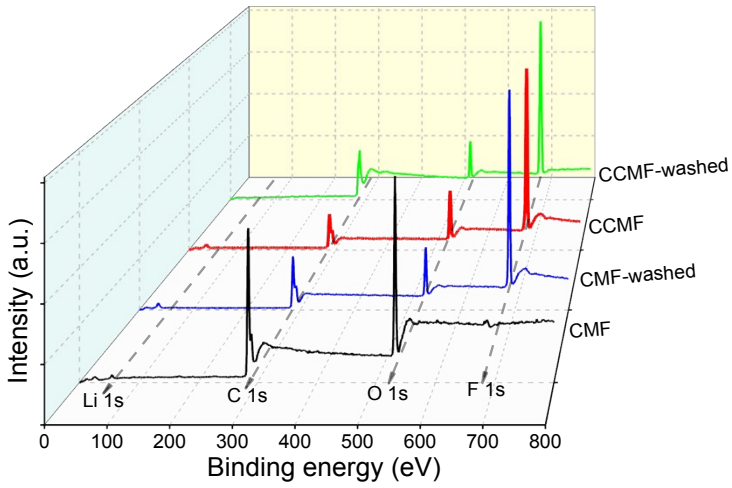

Figure S23. XPS spectra of CMF and CCMF before and after clean electrolyte washing.

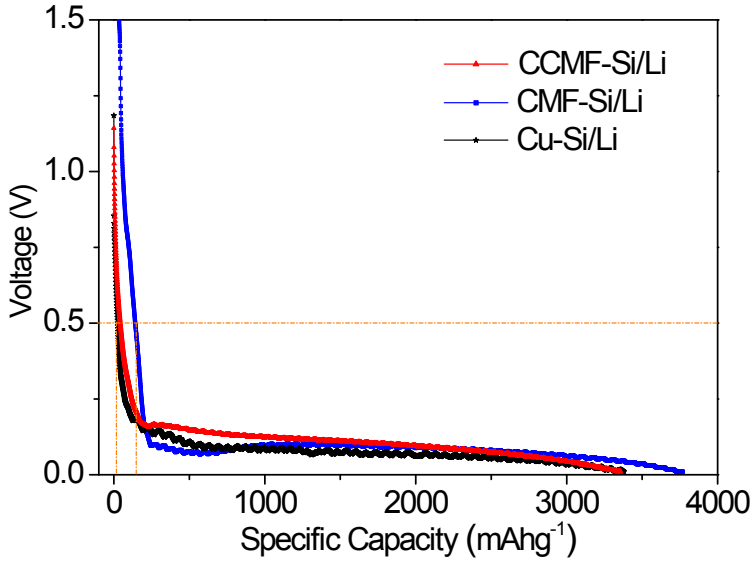

Figure S24. Galvanostatic charge/discharge (0.1 C) at the first cycle of half cells using Si as anode based on the CCMF, CMF and metallic current collectors.

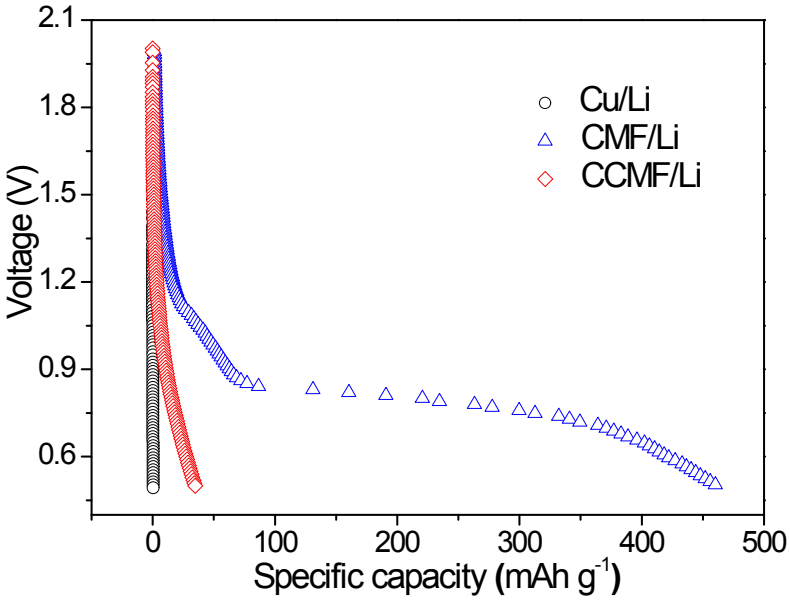

Figure S25. Discharging performance at 0.1 C for the half cells assembled by Cu foil, CMF and CCMF current collectors.

Table S1. The sheet electrical resistance of the Cu foil and CCMF.

Resistance	R1 Ω/sq	R2 Ω/sq	R3 Ω/sq	$R_{average}$
Cu foil	0.1	0.1	0.1	0.1
CMF	1.8	2.0	2.2	2.0
CCMF	2.8	3.5	4.2	3.7

The sheet resistances of Cu foil, CMF and CCMF were measured by a four-probe system, and the last column represents the average values of sheet electrical resistance of the different current collectors. The results indicated CCMF has a higher electrical resistance than that of other substrates.

Table S2. Voltage change (ΔIR) of the Cu-Gra and CCMF-Gra based battery.

Electrode	ΔIR（V）				
	0.5C	**1C**	**2C**	**3 C**	**4C**
Cu-Gra	0.0363	0.0838	0.1386	0.2102	0.2198
CCMF-Gra	0.0198	0.0425	0.0853	0.1228	0.1556
Percentage of drop	45.5 %	49.3 %	38.4 %	41.5 %	29.2 %

Table S3. Comparison of the voltage and actual specific capacity of the foldable battery with other previous flexible batteries.

Battery type	Voltage V	[a]Specific capacity mAh g^{-1}	Active material mass loading mg cm^{-2}	Flexibility	[b]Actual energy density Wh Kg^{-1}
$LiCoO_2$-CNT/$Li_4Ti_5O_{12}$-CNT [3]	2.6	~120	7.2	bending radius <6 mm	108
$LiCoO_2$-CNT-Kimwipe/$Li_4Ti_5O_{12}$-CNT-Kimwipe [4]	~2.5	113	~1	foldable	< 150
$LiCoO_2$-CNT coated/$Li_4Ti_5O_{12}$-CNT coated [5]	2.6	85.5	Not provided	origami	< 150
$LiMn_2O_4$-MWCNT/$Li_4Ti_5O_{12}$-MWCNT [6]	2.75	138	0.12 mg cm^{-1}	flexible	27
$LiFePO_4$-Ni/$Li_4Ti_5O_{12}$-Ni[7]	1.9	81	4	Performance decreased after deformation	< 100
NCA-Al/graphite-Cu [8]	7.4 (two battery connected)	55	11	bending radius 5 mm	< 150
LCO-CC/ FeD-CC [9]	3.4	~80	2	bending angle 90°	< 150
$LiFePO_4$-goldplated PET/$Li_4Ti_5O_{12}$-goldplated PET[10]	2	123	4-5	flexible	< 150
PP-PB-SP/graphite-Cu[11]	3.75	80	0.5-0.8	Performance decreased after deformation	232 (included weight not provided)
$LiCoO_2$-CMF/$Li_4Ti_5O_{12}$-CMF[12]	2.6	150	15	foldable	166
This work	**4.04**	**134**	**15**	**Foldable**	**293**

Note: [a]Specific capacity was read from the literature, which was calculated by the mass of active materials.
[b]Actual energy density was calculated by specific capacity × weight of cathode active matieral × potential plateau / weight of the whole electrodes.

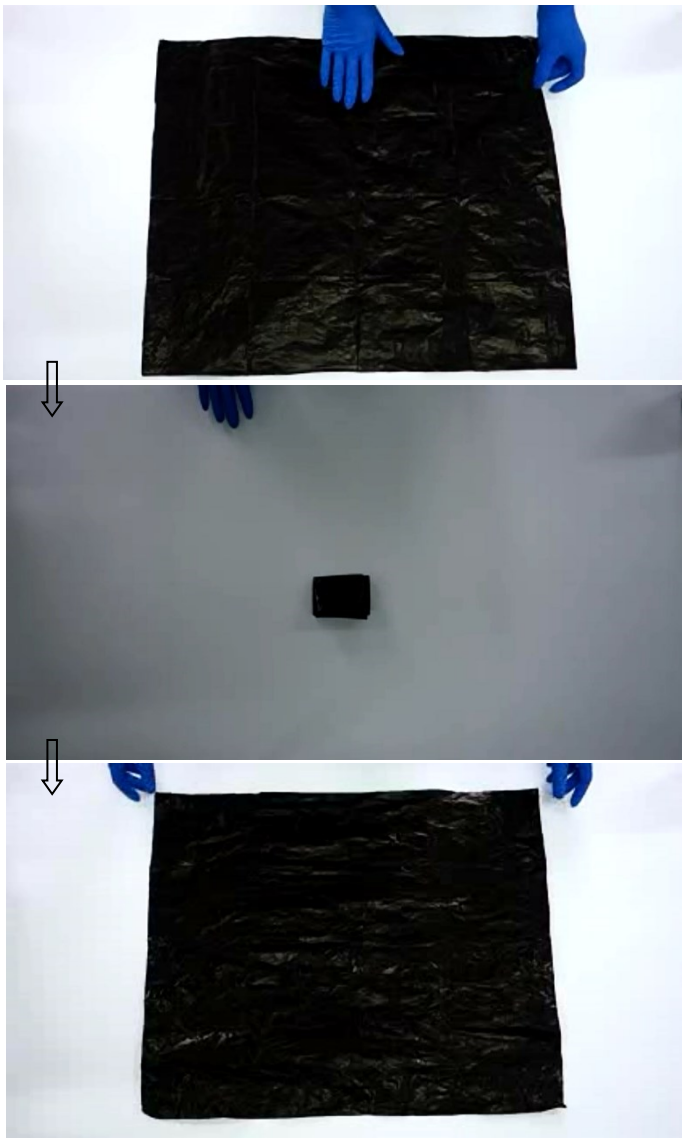

Movie S1. Insensitivity demonstration of the CCMF towards folding and releasing.

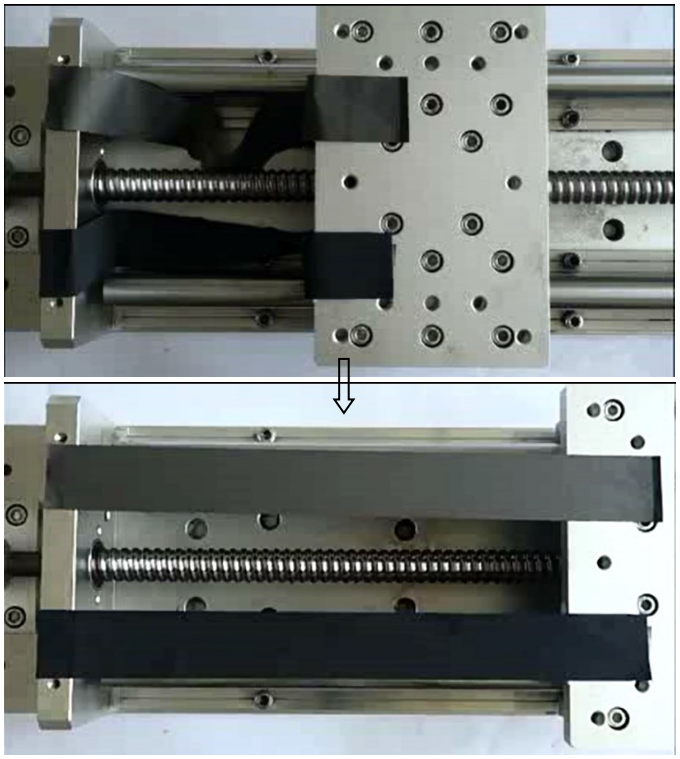

Movie S2. The deformation of cathode and anode electrodes in a linear guide system.

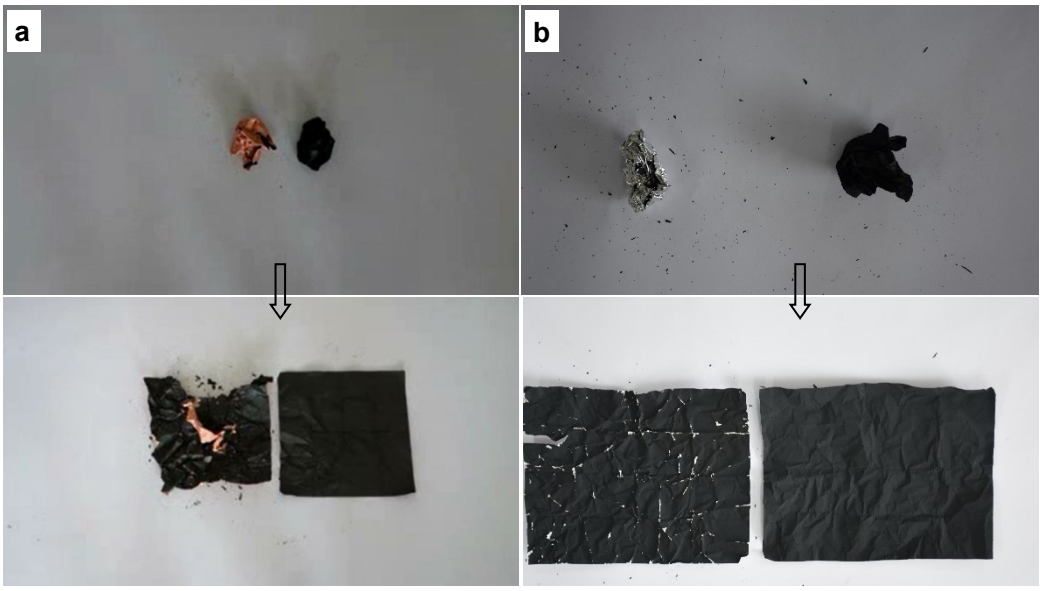

Movie S3. Flexibility demonstration of Cu-Gra (left), CCMF-Gra (right) (a) and Al-LCO (left), CCMF-LCO (right) (b) electrodes.

Movie S4. Open-circuit voltages of foldable CMF-LTO battery.

Movie S5. Open-circuit voltages of foldable CCMF-Gra battery.

Movie S6. LED luminescence response powered by our CCMF-based battery at folding and unfolding.

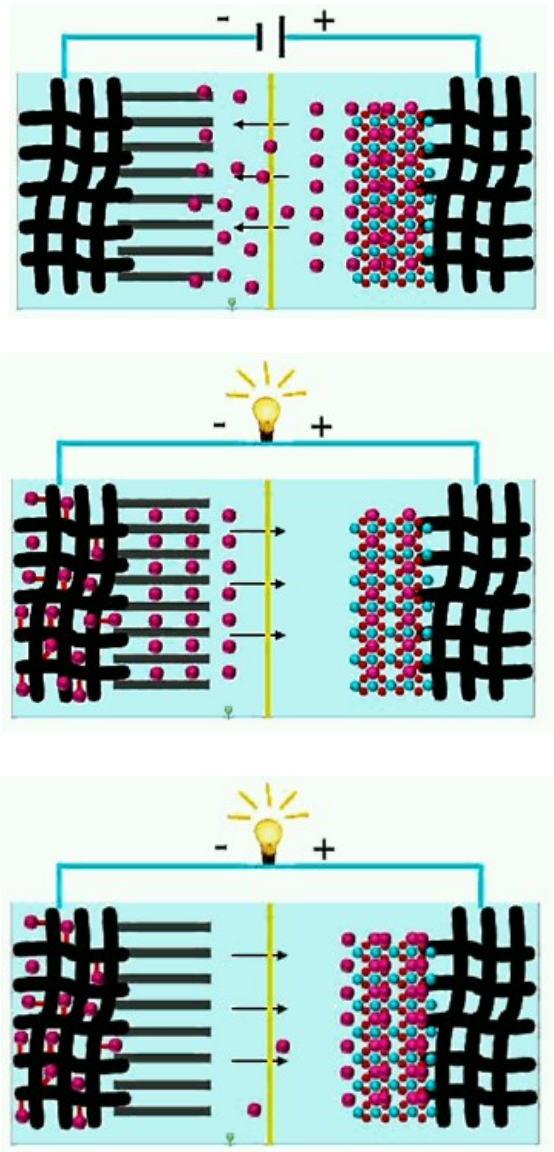

Movie S7. Schematic diagram of lithium ions to intercalate into and de-intercalate from Gra based on CMF.

The movie shows the electrochemical activity of the CMF cannot sidestep the “dangerous region”, where the majority of lithium ions were kept in CNTs and cannot be de-intercalated from CMF electrode. These results demonstrate that the lithium ions in the CNTs will react with carbon atom to form lithium and carbon compound.

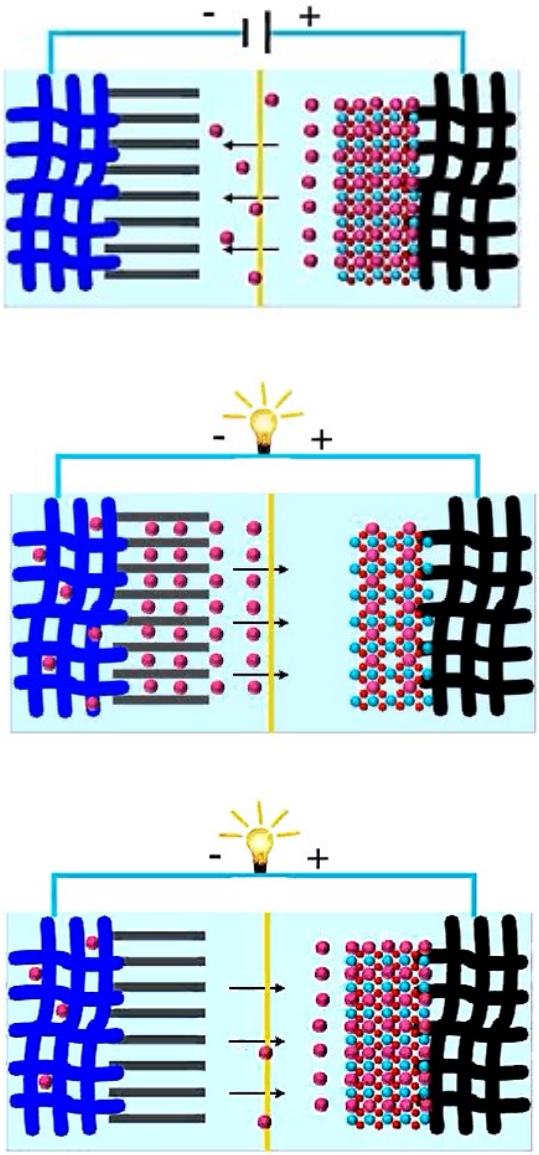

Movie S8. Schematic diagram of lithium ions intercalates into and de-intercalate from Gra based on CCMF.

The movie shows the electrochemical inertness of the CCMF that can avoid the "dangerous region" efficiently, where the majority of lithium ions can intercalate into the CCMF-based electrode and de-intercalate. Due to the potential differences between CCMF and Gra, few lithium ions were remained in CCMF after discharging process without formation of lithium and carbon compound in the system.

References

[1] W. Weppner, R. A. Huggins, Determination of the kinetic parameters of mixted-conducting electrodes and application ot the system Li_3Sb, *J. Electrochem. Soc.*, **1977**,*124*, 1569-1578.

[2] Q. F. Fu, R. J. Li, X. Z. Zhu, G. S. Liang, L. J. Luo, Y. J. Chen, C. F. Lin, X. S. Zhao, Design, synthesis and lithium-ion storage capability of $Al_{0.5}Nb_{24.5}O_{62}$, *J. Mater. Chem, A*, **2019**, *7*, 19862-19872

[3] L. B. Hu, H. Wu, F. L. Mantia, Y. Yang, Y. Cui, Thin, flxeible secondary Li-ion paper batteries, *ACS Nano*, **2010**, *4*, 5843-5848

[4] Q. Cheng, Z. M. Song, T. Ma, B. B. Smith, R. Tang, H. Y. Yu, H. Q. Jiang, C. K. Chan, Folding paper-based liithium-ion batteries for higher areal energy densities, *Nano Lett.*, **2013**, *13*, 4969−4974

[5] Z. M. Song, T. Ma, R. Tang, Q. Cheng, X. WANG, D. Krishnaraju, R. Panat, C. K. Chan, H. Y. Yu, H. Q. Jiang, Origami lithium-ion batteries, *Nat. Commun.*, **2014**, *5*, 3140-1-6

[6] J. Ren, Y. Zhang, W. Y. Bai, X. L. Chen, Z. T. Zhang, X. Fang, W. Weng, Y. G. Wang, H. S. Peng, Elastic and wearable wire-shaped lithium-ion battery with high electrochemical performance, *Angew. Chem. Int. Ed.,***2014**, *53*, 7864-7869

[7] X. Pu, L. X. Li, H. Q. Song, C. H. Du, Z. F. Zhao, C. Y. Jiang, G. Z. Cao, W. G. Hu, Z. L. Wang, A self-charging power unit by integration of a textile triboelectric nanogenerator and a flexible lithium-ion battery for wearable electronics, *Adv. Mater.*, **2015**, *27*, 2472-2478

[8] J. S. Kim, D. Ko, D. J. Yoo, D. S. Jung, C. T. Yavuz, N. I. Kim, I. S. Choi, J. Y. Song, J. W. Choi, A half millimeter thick coplanar flexible battery with wireless recharging capability, *Nano Lett.,* **2015***, 15,* 2350−2357

[9] M. S. Balogun, W. T. Qiu, F. Y. Lyu, Y. Luo, H. Meng, J. T. Li, W. J. Mai, L. Q. Mai, Y. X. Tong, All-flexible lithium ion battery based on thermally-etched porous carbon cloth anode and cathode, *Nano Energy*, **2016**, *26*, 446-455

[10] J. J. Zhang, X. Zang, H. J. Wen, T. T. Dong, J. C. Chai, Y. Li, B. B. Chen, J. W. Zhao, S. M. Dong, J. Ma, L. P. Yue, Z. H. Liu, X. G. Guo, G. L. Cui, L. Q. Chen, High-voltage and free-standing poly(propylene carbonate)$Li_{6.75}La_3Zr_{1.75}Ta_{0.25}O_{12}$ composite solid electrolyte for wide temperature range and flexible solid lithium ion battery, *J. Mater. Chem. A*, **2017**, *5*, 4940-4948

[11] Y. H. Zhu, X. Yang, D. Bao, X. F. Bie, T. Sun, S. Wang, Y. S. Jiang, X. B. Zhang, J. M. Yan, Q. Jiang, High-energy-density flexible potassium-ion battery based on patterned electrodes, *Joule*, **2018**, *2*, 736-746

[12] T. Liu, M. Zhang, Y. L. Wang, Q. Y. Wang, C. Lv, K. X. Liu, S. Suresh,Y. H. Yin,Y. Y. Hu, Y. S. Li, X. B. Liu, S. W. Zhong, B. Y. Xia, Z. P. Wu, Engineering the surface/interface of horizontally oriented carbon nanotube macrofilm for foldable lithium-ion battery withstanding variable weather, *Adv. Energy Mater.*, **2018**, *8*, 1802349-1-10